UV-A Estimation in Atacama Desert from GHI Measurements by Using Artificial Neural Network

Gino Mondaca[1], Mauricio Trigo-González[1], Aitor Marzo[1], Joaquín Alonso-Montesinos[2], Javier Barbero[2], Germán Salazar[3], Douglas Olivares[1] and Pablo Ferrada[1]

[1] Centro de Desarrollo Energético Antofagasta, Universidad de Antofagasta, Antofagasta (Chile)

[2] CIESOL, Joint Centre of the University of Almeria-CIEMAT, Almería (España)

[3] Departamento de Física, Universidad Nacional de Salta, Salta Capital (Argentina)

Abstract

The Atacama Desert presents ideal conditions for the proliferation of solar projects due to the high solar resource present in the area. However, Atacama Desert is also known to have a large amount of ultraviolet radiation due to the scarcity of ozone and aerosols in its atmosphere. Ultraviolet radiation is harmful to the people who work under its influence and affects the durability of the materials used in PV facilities. Two useful models for the estimation of solar irradiance and daily solar irradiation in the ultraviolet A spectral range in the Atacama Desert are shown in this paper. The models were generated by using artificial neural networks and use global horizontal irradiance measurements and astronomical calculations as inputs. Results show relative errors of 6% and 3% for the estimations of UV-A irradiance and UV-A daily irradiation, respectively. Therefore, these models show that they are reliable for the estimation of solar radiation in the UV-A range in the Atacama Desert, being able to provide information in those places where it is needed.

Keywords*: UV-A irradiance, artificial neural network, Atacama Desert, Resource solar*.

1. Introduction

Nomenclature

Abbreviations		Symbol	Meaning	Units
PSDA	Plataforma Solar del Desierto de Atacama	GHI	Global Horizontal Irradiance	[W m^{-2}]
ANN	Artificial Neural Network	WS	Wind speed	[m/s]
CDEA	Centro de Desarrollo Energético Antofagasta	T_{air}	Ambient Temperature	[°C]
LMA	Levenberg-Marquardt Algorithm	RH	Relative Humidity	[%]
MSE	Mean Square Error	P_{atm}	Atmospheric Pressure	[mb]
MBE	Mean Bias Error	UV-A	Ultraviolet Type A	-
RSME	Root Mean Square Error	SZA	Solar Zenith Angle	[°]
		AM	Air Mass	[NU]

Ultraviolet solar radiation (UV) is part of the solar radiation that reaches the Earth's surface. Specifically, UV is defined as the spectral range between the 200 nm and 400 nm wavelengths of the electromagnetic spectrum. This spectral range is the one in which the most energetic photons reach the earth's surface. According to the spectral sub-band, it is named as UV-A, UV-B, and UV-C for the 315-400 nm, 280-315 nm, and 200-280 nm ranges, respectively. Its intensity is influenced by several factors, such as, sun elevation, geographical parameters, clouds, and atmospheric aerosol and ozone content. It contents the 4.6% of the energy coming from sunlight under standard conditions, according to the standard solar spectrum (ASTM G173).

The health damage caused by ultraviolet radiation is well known, as it is highlighted in the INTERSUN program of the World Health Organization. This program aimed urgently to undertake research into the effects on human health of the increase in ultraviolet radiation and to study the possibility of taking appropriate corrective measures. However, ultraviolet radiation does not only affect human health. Materials made of natural or synthetic polymers can be affected by ultraviolet radiation when exposed to sunlight. This reduces the durability of products using these materials, a problem known as UV degradation (Leun et al., 1995)(Kowalski, 2009)(Andrady et al., 1998).

In the context of photovoltaic (PV) technologies, UV solar radiation can affect in different ways. For instance, PV cells are composed of a crystal that protects them from external conditions, an encapsulant and the photodiode where the energy of the photons is transformed into electrical energy. Encapsulants are needed to provide electrical

doi:10.18086/swc.2019.08.08 Available at http://proceedings.ises.org

insulation and to protect modules from mechanical damage and environmental corrosion (Kempe, 2008). They usually consist of polymers that are affected by UV radiation, in combination with other parameters, reducing their transparency. A reduction in the encapsulant transparency means a reduction of the amount of solar radiation reaches PV cells and, consequently, the efficiency of the modules (Rosenthal and Lane, 1991)(Wenger et al., n.d.)(Wenger et al., n.d.)(Jordan and Kurtz, 2012).

However, the effect of UV radiation can also be used to favor certain processes of interest. Specifically, water treatments, such as solar disinfection or photocatalysis, are current methods based on the use of solar UV radiation for the treatment of drinking water (Pichel et al., 2019)(Mark D. Sobsey, 2002) (Chong et al., 2010). These water treatment technologies are of special interest in places where drinking water is scarce and there is a high solar resource, such as the desert areas of the planet, mainly located in the sun belt.

Due to all this, information about the amount of UV radiation in a certain place, is essential for several scientific disciplines.

In the area of machine learning, the algorithm of artificial neural network (ANN) is divided into the important areas of learning, are supervised learning, unsupervised learning and reinforced learning. In this work, it is focused on supervised learning, mixing statistical indicators in order to obtain a one-layer network for a model that takes into account the balance of few variables and a low estimation error of irradiance UV-A.

2. Emplacement and instrumentation

The Plataforma Solar del Desierto de Atacama (PSDA) belongs to the Centro de Desarrollo Energético Antofagasta (CDEA) of the University of Antofagasta. The PSDA is a natural laboratory where solar technologies are tested under the extreme conditions of aridity and high radiation of Atacama (Olivares et al., 2017). It is located at 24.09°S, 69.93°W and 1000 m of altitude, near the Aguas Blancas basin, at 80 km southeast of the city of Antofagasta.

Fig.1 (a) shows the PSDA geographical location and Fig.1 (c) shows an overview of the PSDA facilities. The most relevant facility for this paper is its meteorological station, shown in Fig.1 (b). In this station, meteorological and solar radiation parameters are measured. Instrumentation is maintained daily by PSDA operation staff. Average, maximum and minimum values of the measurements are recorded with a time resolution of 1 minute in dataloggers and a computer. Every night, the computer sends the data to a remote server where it is stored.

Fig. 1: (a) location of the PSDA. (b) Close perspective of PSDA meteorological station. (c) Global view of PSDA

The instrumentation used in this paper is described in table 1. The data used in this paper corresponds to the time period from April 27, 2017 to January 31, 2019.

Table 1 instrumentation and variables available at PSDA and used in this paper

Variable	Instrument
GHI	Kipp&Zonen CMP22
WS	Young 05103
T_{air}	Campbell Scientific HMP60
RH	Campbell Scientific HMP60
P_{atm}	Campbell Scientific CS106
UV-A	Kipp&Zonen UVS-AB

3. Methodology

In this paper, two artificial neural network with supervised learning were designed for the development of the two UV-A radiation models. The first model estimates the surface density power received on a horizontal surface, irradiance, in [W m^{-2}]. The second model allows to estimate the radiative energy received on a horizontal surface along a day, daily irradiation, in [Wh m^{-2}].

An ANN consists of a set of units, called artificial neurons, connected together to transmit signals. The input information passes through the neural network (where it undergoes several operations) producing output values. There are two types of classification and regression, in this case the regression will be used. Fig. 2 shows a general scheme of an ANN

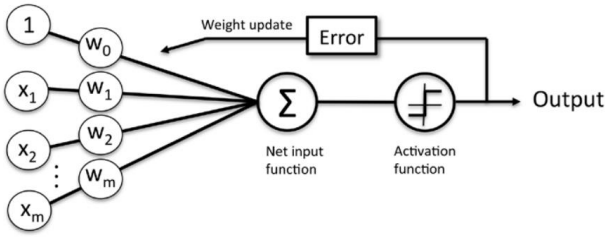

Fig. 2: Generic diagram of an artificial neuronal network (Raschka, 2015)

An important criterion for the input choice of an ANN is the number of configurations. the input configuration is described by 2^n, where n is the number of inputs. If there is no relevant input configuration in the network output, a physical criterion is used for a new configuration.

The backpropagation algorithm of *Levenberg-Marquardt* (LMA) (Marquardt, 1963) Eq. 1 was used. The advantage of this algorithm is that they converge in the fastest MSE compared to other algorithms (decreasing gradient). This equation updates the weights of the neural network where w is the weight of each neuron, α is the training rate, j is the jacobian error matrix of the output neurons, e is the error of the vector output, μ damping factor and I identity matrix.

$$w(n+1) = w(n) - \alpha * w(n-1) - \frac{J^T * e}{J^T * J + \mu * I} \qquad \text{(eq. 1)}$$

Joint data (measured data and additional variables) were used in the development of the artificial neural network. The data were separated into 2/3 (training) and 1/3 (validation). Internally, the Matlab program uses the MSE as an indicator of learning performance of ANNs.

To evaluate the models performed by the developed neural networks, the MBE (Mean bias error) and RSME (Root mean square error) were applied according to eq.2 and eq.3, where n is the number of data, UV-A_e estimated irradiance and UV-A_m measured irradiance. this same equation is applied for the validation of the daily UV-A irradiation model.

$$MBE\ (\%) = 100 * \frac{1}{n} \sum_{i=1}^{n} \frac{UVA_e - UVA_m}{UVA_m} \qquad \text{(eq. 2)}$$

$$RMSE\ (\%) = 100 * \sqrt{\frac{1}{n} \sum_{i=1}^{n} \left(\frac{UVA_e - UVA_m}{UVA_m} \right)^2} \qquad \text{(eq. 3)}$$

To develop the models, measurements shown in Table 1 were used. Additionally, declination (δ), solar zenith angle (SZA) and its cosine, air mass (AM), extraterrestrial irradiance (I_{ext}) and clearness index (K_T), we call astronomical variables, were calculated and included as inputs for the ANN.

Declination (δ) is calculated according to *Spencer* (perpiñan lamigueiro, 2013), Eq. 4 and Eq. 5.

$$\Gamma = 2 * \pi * (d_n - 1)/365 \qquad \text{(eq. 4)}$$

$$\delta = 0{,}006918 - 0{,}399912 * \cos(\Gamma) + 0{,}070257 * -0{,}006758 * \cos(2\Gamma) + 0{,}000907 * \sin(2\Gamma) - 0{,}002697 * \cos(3\Gamma) + 0{,}001480 * \sin(3\Gamma) \quad \text{(eq. 5)}$$

Where Γ is the day angle, in radians, and d_n is the day number of the year, ranging from 1 on 1 January to 365 on 31 December (Muhammad Iqbal, 1983). SZA is calculated according the following expression:

$$cos\, S\, ZA = sin\delta\, sin\varphi + cos\, \delta\, cos\, \varphi\, cos\, \omega \quad \text{(eq. 6)}$$

Being φ and ω the local latitude and the hour angle, respectively. AM can now be calculating with the following approximation:

$$AM = \frac{1}{\cos(SZA)} \quad \text{(eq. 7)}$$

I_{ext} is estimated according to the solar constant I_0 and the eccentricity (E):

$$I_{ext} = I_0 \left(\frac{r_0}{r}\right)^2 = I_0\, E \quad \text{(eq. 8)}$$

Where r_0 and r are the average distance and the real distance between earth and sun, and E is calculated according to:

$$E = \left(\frac{r_0}{r}\right)^2 = (1.00011 + 0.034221 \cos\Gamma + 0.00128 \sin\Gamma + 0.000719 \cos 2\Gamma + 0.000077 \sin 2\Gamma)^{-1} \quad \text{(eq. 9)}$$

KT can be used to classify cloudy days in three types, as clear, partially cloudy or cloudy days. The latter provides information that can give indications of the learning trend that the artificial neural network may have.

To calculate the clearness index Eq.10 is used, where K_T is the clearnessness index, GHI is the horizontal global irradiance and I_{ext} is the extraterrestrial irradiance (W m^{-2}). According to Iqbal criteria (Muhammad Iqbal, 1983), the value of K_T maybe used to classify the day as clearness $0.65 < K_T \leq 0.9$; partly cloudy $0.3 < K_T \leq 0.65$; cloudy $0 \leq K_T \leq 0.3$.

$$K_T = \frac{GHI}{I_{ext}} \quad \text{(eq. 10)}$$

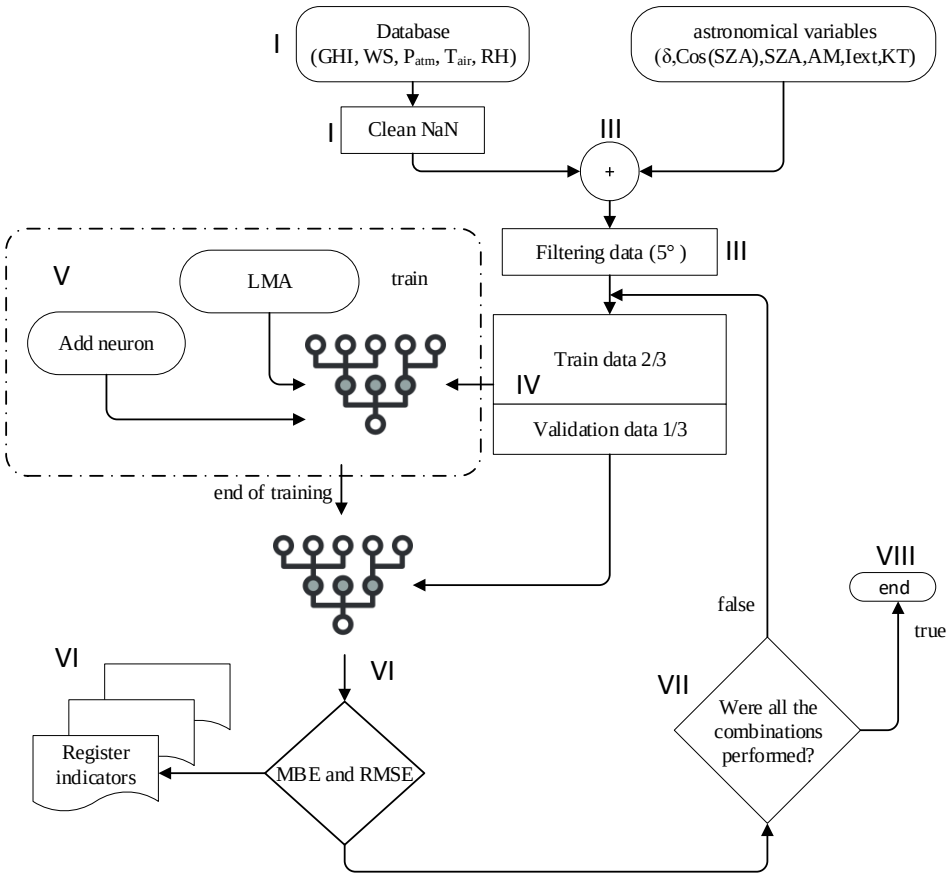

Fig. 3: Flow diagram of the methodology

Fig. 3 shows a diagram of data processing and the methodology applied to develop the ANN model. Each step is explained below:

i. The measurement database (GHI, WS, P_{atm}, T_{air}, RH) is processed to eliminate NAN type data that negatively influence the model.
ii. The astronomical variables are calculated and added to the database (δ, $cos\,SZA$, SZA, AM, I_{ext}, K_T).
iii. The nocturnal data is deleted from the database. For this purpose, the data corresponding to SZA > 85° are deleted.
iv. The resulting database is then divided into two groups: 2/3 for ANN training and 1/3 will for ANN validation.
v. In this point the ANN training is preformed, starting with 2 neurons and with the combination of selected variables (see table 4 and 5). At this stage, the *Levenberg-Marquardt* learning algorithm (LMA) is used in combination with the MSE as performance indicator. The algorithm seeks to reduce to minimum the MSE in this learning period.
vi. Once the training is finished, RMSE and MBE are obtained and recorded for later analysis.
vii. This step controls whether all variable combinations (tables 4 and 5) have already been considered in the training and validation stages. If any combination remains, then step v is started with that combination.
viii. Finally, the optimal model is chosen, verifying the results with the values of RMSE and MBE.

4. Results y discussion

This section presents the results obtained for ultra-violet ANN models of irradiance and daily irradiation. Before carrying out any ANN training and validation, it is important to consider the nature of the data. For that end, K_T is used to classify the day as clear, partially cloudy and cloudy, according Iqbal criteria. For irradiance measurements, the 81% of the measurements were performed under clear sky conditions, the 17% under partially cloudy conditions and the remaining 2% under cloudy conditions. Therefore, the ANN will have a learning tendency towards clear days.

4.1 Results of the ANN training and validation stages

Once the data has been processed, the RMSE and MBE are obtained. Table 2 shows the results of the different variable combination used for the UV-A irradiance ANN model.

Table 2 RMSE and MBE artificial neural network for instant UV-A irradiance

Model	GHI [W/m2]	WS [m/seg]	T_{air} [°c]	RH [%]	P_{atm} [Atm]	δ [°]	cos(SZA) []	SZA [°]	AM [NU]	I_{ext} [W/m2]	K_T [NU]	RMSE (%)	MBE (%)
01	x	x	x	x	x	x	x	x	x	x	x	5.72	0.00
02		x	x	x	x	x	x	x	x	x	x	5.72	0.01
03	x		x	x	x	x	x	x	x	x	x	5.73	0.01
04	x	x		x	x	x	x	x	x	x	x	5.88	-0.01
05	x	x	x		x	x	x	x	x	x	x	5.72	-0.01
06	x	x	x	x		x	x	x	x	x	x	5.74	-0.01
07	x	x	x	x	x		x	x	x	x	x	5.86	0.00
08	x	x	x	x	x	x		x	x	x	x	5.73	0.01
09	x	x	x	x	x	x	x		x	x	x	5.72	0.01
10	x	x	x	x	x	x	x	x		x	x	5.72	0.00
11	x	x	x	x	x	x	x	x	x		x	5.73	0.00
12	x	x	x	x	x	x	x	x	x	x		5.85	0.02
13	x	x	x	x	x							7.01	0.02
14	x						x			x	x	6.02	0.00
15	x			x			x		x	x	x	5.90	0.01
16	x		x	x	x		x			x	x	5.85	0.01
17	x					x	x				x	5.97	-0.02
18	x						x	x		x		5.55	0.00
19	x							x		x		5.58	-0.01
20	x						x			x		5.61	0.02
21								x		x		9.43	0.03

On one hand, model 1 is the one that considers all the available variables. Its RMSE value was 5.72% and the MBE was 0%. On the other hand, the models from 2 to 12, consider all variables except one of them. The RMSE results were close to 6% while the MBE value was negligible.

Subsequently, the combinations of variables were selected by using a physical criteria. The GHI is considered in all the following models, because the UV-A radation is a part of the GHI spectrum. Model 13 only take into account the measurements, resulting in the highest RMSE% value, 7.01%. This indicates that the astronomical parameters and the K_T are important for the development of the model. Model 14 was performed considering the GHI, cos SZA, Iext and K_T. Models 15 and 16 were more centered on variables that maybe involved in the definition of atmospheric conditions, such us T_{air}, RH, and P_{atm}. Their RMSE and MBE values were arround 5.87% and 0.01%, respectively. Model 17 only considers astronomical variables, where its error is close to 6%. Model 18 considers only GHI and Iext, as well as SZA and its cosine. This model obtain the lowest RMSE with a value of 5.55%. Models 19 and 20 attempt to quantify the influence of the solar zenith angle and its cosine, demonstrating that the contribution of the cosine is less compared to the angle. The RMSE and MBE values for model 19 and 20 were 5.58% and 5.61% and -

0.01% and 0.02%, respectively. Finally, model 21 shows that the absence of the GHI affects the model to a great extent by raising the RMSE to 9.43%.

From the results, model 20 was selected taking into account its RMSE and MBE values and the number of input variables.

In the case of daily UV-A irradiation, the same criteria were considered for the choice of inputs combinations. Table 3 shows the inputs combination and its respective RMSE and MBE values. GHI_d and $I_{ext,\,d}$ were calculated from GHI and Iext values. WS_d, $T_{airc,\,d}$, RH_d, $P_{atm,d}$ were daily averages of the measurement. SZA was considerd at noon.

Table 3 RMSE and MBE artificial neural network for daily UV-A irradiation

Model	GHI_d [Wh/m2]	WS_d [m/seg]	$T_{airc,\,d}$ [°C]	RH_d [%]	$P_{atm,d}$ [Atm]	δ [°]	cos(SZA) [NU]	SZA [°]	AM [NU]	$I_{ext,\,d}$ [Wh/m2]	K_T [NU]	RMSE (%)	MBE (%)
01	x	x	x	x	x	x	x	x	x	x	x	2.53	0.05
02		x	x	x	x	x	x	x	x	x	x	2.53	-0.13
03	x		x	x	x	x	x	x	x	x	x	2.45	0.01
04	x	x		x	x	x	x	x	x	x	x	2.69	-0.09
05	x	x	x		x	x	x	x	x	x	x	2.93	6.89
06	x	x	x	x		x	x	x	x	x	x	3.16	0.24
07	x	x	x	x	x		x	x	x	x	x	2.58	0.12
08	x	x	x	x	x	x		x	x	x	x	2.68	0.03
09	x	x	x	x	x	x	x		x	x	x	2.72	-0.06
10	x	x	x	x	x	x	x	x		x	x	2.46	-0.04
11	x	x	x	x	x	x	x	x	x		x	2.49	1.48
12	x	x	x	x	x	x	x	x	x	x		2.53	-0.13
13	x	x	x	x	x							2.77	0.01
14	x						x			x	x	3.23	0.19
15	x			x			x		x	x	x	2.65	0.09
16	x		x	x	x		x			x	x	2.75	0.00
17	x					x	x				x	2.56	0.16
18	x					x	x	x		x		2.55	0.12
19	x					x				x		2.81	0.44
20	x							x		x		2.86	0.05
21	x						x			x		2.61	0.11
22						x	x	x		x		5.60	-0.40

As in the previous case, model 1 is ANN in which all available variables are used. Models 2 to 12 are those in which only one variable is eliminated and models 13 to 17 use physical criteria, the latest model being 18 being the optimum case. It should be noted that in this case declination plays an important role in the performance of the models, since it is related to the angle of incidence of the sun's rays on the earth's surface.

In general, the RMSE of irradiation models has been halved compared to irradiance models. That is, from an average of 6% for all irradiance cases, to an average of 3% for irradiation.

The best results were obtained for model 18. This model uses exclusively GHI_d measurements and considers the **δ**, $I_{ext,\,d}$, SZA and cos SZA variables.

4.2 Analysis of variables of the chosen models

In order to better understand the role that these variables play in the estimation of irradiance, the data of the variables chosen for both models are collated with respect to the values of irradiance and irradiation UV-A. The results are presented in Figures 4 and 5, respectively.

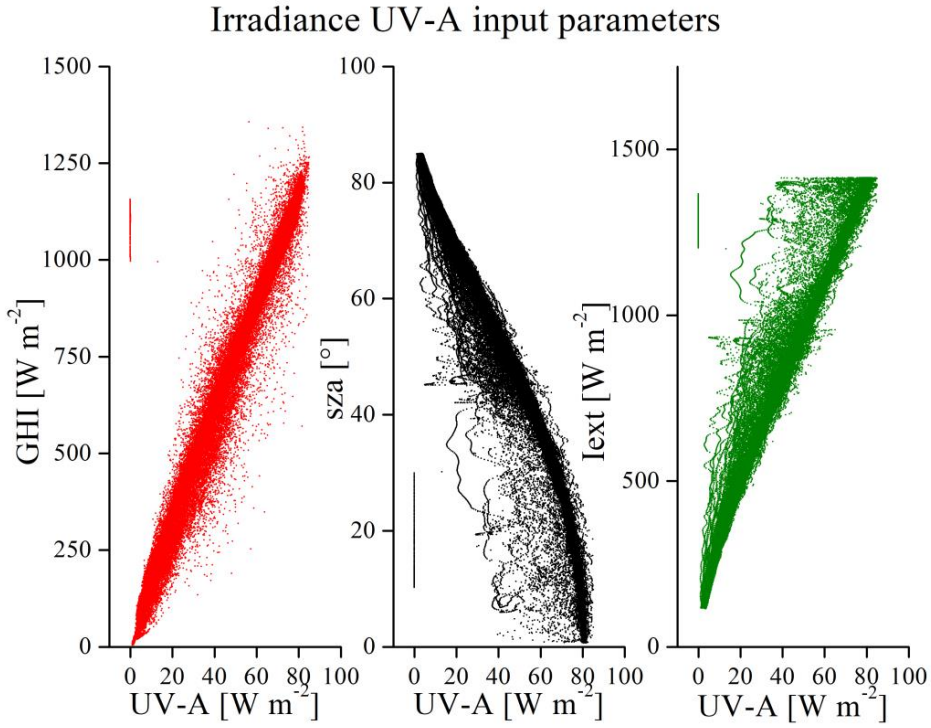

Fig. 4: comparison of variables with UV-A irradiance

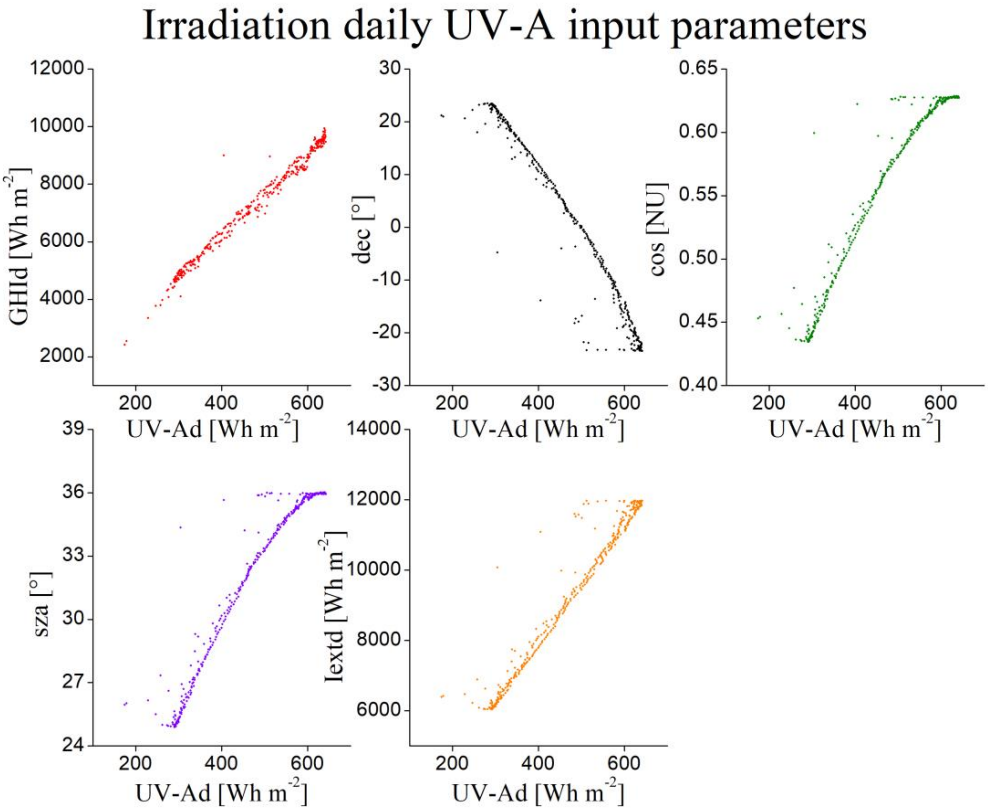

Fig. 5: Comparison of variables with daily UV-A irradiation

Figure 4 shows the results of the variables used for the UV-A irradiance model. All three variables present linearity with UV-A with Pearson coefficient values of 0.99 for GHI, 0.98 for SZA and 0.98 for I_{ext}. However, the variables SZA and I_{ext} show some diffusion of points towards low UV-A values. This is due to the presence of a few data

measured on partially cloudy days. In future work, the development of models based on sky conditions will be considered in order to improve the results.

The results obtained for the variables included in the daily irradiation model are shown in Figure 5. Since these are daily data, the amount of data available is much lower than that of the irradiance measurements. As in the previous case, all the variables considered in the model show a linear relationship with the UV-A irradiation. The Pearson coefficient values obtained in this case were 0.99 for GHI_d, -0.97 for dec, 0.97 for cos SZA, 0.97 for SZA and 0.97 for $I_{ext,d}$. It is important to point out that in the case of declination its slope is negative, since the place of measurements is located in the southern hemisphere.

4.3 Selected model validation

As explained above, the artificial neural network is constructed from the selected combination of inputs and varying the number of hidden neurons, up to a maximum of 10. For this, the MLA is used in order to reduce MSE.

For the validation phase, 1/3 of the data not used in the training phase is used now. From these validation stage, RMSE and MBE are calculated, as shown in tables 2 and 3. The results of the validation stage for the two selected irradiance and irradiation models are shown in more detail below.

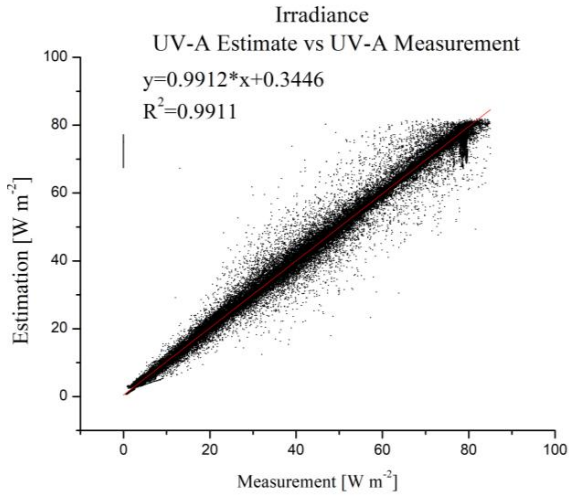

Fig. 6 UV-A irradiance measurement vs estimation.

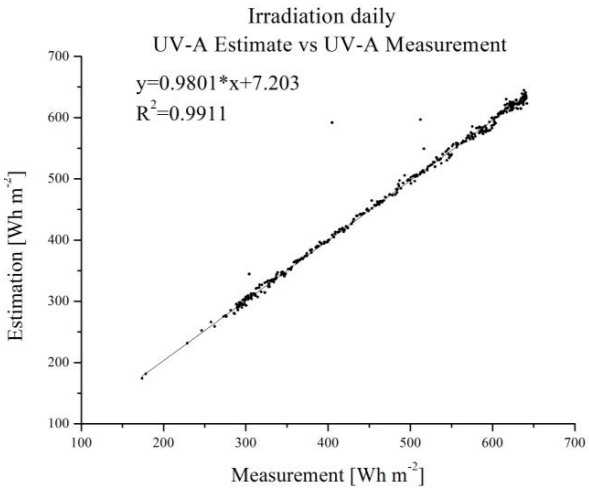

Fig. 7 UV-A daily irradiation measurement vs estimation.

Fig. 6 shows the scatter plot of the validation stage for the UVA irradiance model number 19. The model uses GHI, cos SZA and Iext as inputs. The network consists of 10 hidden neurons. The graph shows the UVA irradiance estimates versus the measurements. The value of RMSE was 5.61% and MBE 0.02%. Fig. 6 shows the linear fit of the estimated vs. measured data. Its quadratic error was 0.99. The good fit of the model agrees with the results obtained with the RMSE and MBE errors.

Figure 7 shows the scatter plot of the validation of the daily UVA irradiation model number 18. The selected model uses values of GHId, dec, SZA, cos SZA, Iextd. The resulting RMSE and MBE values were 2.55% and 0.12%, respectively. The data from the model and the measurements showed a good linear fit as shown in fig.8. The quadratic fit error was 0.99.

for future work, the search for UVA databases and parameters of interest in the Atacama Desert is being carried out for the development of the model. Likewise, the methodology proposes the use of kernel (Habte et al., 2019)(Deo et al., 2017) that group the variables as new input. Models will also be developed according to the conditions of clear, partially cloudy and cloudy skies.

5. Conclusion

In this work, two models have been created for the estimation of daily irradiance and UVA irradiation, using neural networks and data measured at the PSDA meteorological station. For this purpose, an analysis was made of the different available variables, selecting the best combination of them, trying to minimize the number of inputs and the RMSE and MBE.

The final UVA irradiance model uses GHI, SZA and I_{ext} as inputs and 10 hidden neurons. The results of the RMSE and MBE were 5.61% and 0.02%, respectively. The selected UVA daily irradiation model uses GHI, dec, cos, SZA and I_{ext} variables as inputs and also 10 hidden neurons. In that case, the RMSE and MBE values were 2.55% and 0.12%. As these results show, both models agree with the measurement and show a good lineal fit with a quadratic error, R^2, of 0.99.

The most relevant result of this work is that it has been possible to develop two models for the estimation of irradiance and UVA irradiation using exclusively the measurements of horizontal global irradiance carried out with a pyranometer and calculations linked to the position of the sun. The results showed that both models are reliable and can be used to estimate UVA radiation in the study area.

It remains pending for the improvement of the models, to include in the development of the same information of other places in the Atacama Desert. We are also seeing the possibility of generating the models considering the sky conditions and the use of new statistical techniques such as the grouping of the variables in kerners for the training of the networks.

6. Acknowledgements

The authors acknowledge FONDECYT Project N°11190289 "Performance Analysis of Photovoltaic Materials and Devices exposed to Ultraviolet Light of Atacama Desert", the Chilean Economic Development Agency (CORFO) with contract No 17PTECES-75830 under the framework of the project “AtaMoS TeC”, the generous financial support provided by the Innova Chile - CORFO, project code: 17BPE3-83761, and the generous financial support provided by the GORE-Antofagasta, Chile, Project FIC-R Antofagasta 2017 BIP code 30488824-0 and the CONICYT/FONDAP/15110019 “Solar Energy Research Center” SERC-Chile. Authors also would like to thank the the PVCastSOIL Project (ENE2017-83790-C3-1, 2 and 3), which was funded by the Ministerio de Economía y Competitividad and co-financed by the European Regional Development Fund.

7. References

Andrady, A.L., Hamid, S.H., Hu, X., Torikai, A., 1998. Effects of increased solar ultraviolet radiation on materials. J. Photochem. Photobiol. B. 46, 96–103.

Chong, M.N., Jin, B., Chow, C.W.K., Saint, C., 2010. Recent developments in photocatalytic water treatment technology: A review. Water Res. 44, 2997–3027. https://doi.org/10.1016/J.WATRES.2010.02.039

Das, U.K., Tey, K.S., Seyedmahmoudian, M., Mekhilef, S., Idris, M.Y.I., Van Deventer, W., Horan, B., Stojcevski, A., 2018. Forecasting of photovoltaic power generation and model optimization: A review. Renew. Sustain. Energy Rev. 81, 912–928. https://doi.org/10.1016/j.rser.2017.08.017

Deo, R.C., Downs, N., Parisi, A. V., Adamowski, J.F., Quilty, J.M., 2017. Very short-term reactive forecasting of the solar ultraviolet index using an extreme learning machine integrated with the solar zenith angle. Environ. Res. 155, 141–166. https://doi.org/10.1016/j.envres.2017.01.035

Habte, A., Sengupta, M., Gueymard, C.A., Narasappa, R., Rosseler, O., Burns, D.M., 2019. Estimating ultraviolet radiation from global horizontal irradiance. IEEE J. Photovoltaics 9, 139–146. https://doi.org/10.1109/JPHOTOV.2018.2871780

Jordan, D.C., Kurtz, S.R., 2012. Photovoltaic Degradation Rates -- An Analytical Review: Preprint.

Kempe, M.D., 2008. Accelerated UV Test Methods for Encapsulants of Photovoltaic Modules. 33rd IEEE 5.

Kowalski, W., 2009. UV Effects on Materials, in: Ultraviolet Germicidal Irradiation Handbook. Springer Berlin Heidelberg, Berlin, Heidelberg, pp. 361–381. https://doi.org/10.1007/978-3-642-01999-9_15

Leun, J.C. van der, Tang, X., Tevini, M., 1995. Environmental effects of ozone depletion: 1994 assessment, Ambio.

Mark D. Sobsey, 2002. Managing Water in the Home: Accelerated Health Gains from Improved Water Supply Water, Sanitation and Health Department of Protection of the Human Environment World Health Organization Geneva.

Marquardt, D., 1963. An Algorithm for Least-Squares Estimation of Nonlinear Parameters. SIAM J. Appl. Math. Vol. 11 No, 431–441.

Muhammad Iqbal, 1983. An Introduction to Solar Radiation, An Introduction to Solar Radiation. Academic Press. https://doi.org/https://doi.org/10.1016/B978-0-12-373750-2.X5001-0

Olivares, D., Ferrada, P., Matos, C. de, Marzo, A., Cabrera, E., Portillo, C., Llanos, J., 2017. Characterization of soiling on PV modules in the Atacama Desert. Energy Procedia 124, 547–553. https://doi.org/10.1016/j.egypro.2017.09.263

perpiñan lamigueiro, O., 2013. Energia Solar Fotovoltaica.

Pichel, N., Vivar, M., Fuentes, M., 2019. The problem of drinking water access: A review of disinfection technologies with an emphasis on solar treatment methods. Chemosphere 218, 1014–1030. https://doi.org/10.1016/J.CHEMOSPHERE.2018.11.205

Raschka, S., 2015. Python Machine Learning Essentials. https://doi.org/10.1017/CBO9781107415324.004

Raza, M.Q., Nadarajah, M., Ekanayake, C., 2016. On recent advances in PV output power forecast. Sol. Energy 136, 125–144. https://doi.org/10.1016/j.solener.2016.06.073

Rosenthal, A.L., Lane, C.G., 1991. Field test results for the 6 MW Carrizo solar photovoltaic power plant. Sol. Cells 30, 563–571. https://doi.org/10.1016/0379-6787(91)90088-7

Wenger, H.J., Jennings, C., Iannucci, J.J., n.d. Carrisa Plains PV power plant performance, in: IEEE Conference on Photovoltaic Specialists. IEEE, pp. 844–849. https://doi.org/10.1109/PVSC.1990.111740

Wenger, H.J., Schaefer, J., Rosenthal, A., Hammond, B., Schlueter, L., n.d. Decline of the Carrisa Plains PV power plant: the impact of concentrating sunlight on flat plates, in: The Conference Record of the Twenty-Second IEEE Photovoltaic Specialists Conference - 1991. IEEE, pp. 586–592. https://doi.org/10.1109/PVSC.1991.169280